

The Formation of Clusters and Nanocrystals in Er-Implanted Hexagonal Silicon Carbide

U. Kaiser,^{1*} D.A. Muller,² A. Chuvilin,³ G. Pasold,¹ and W. Witthuhn¹

¹*Institut für Festkörperphysik, Friedrich-Schiller-Universität Jena, Max-Wien-Platz 1, D-07743 Jena, Germany*

²*Bell Laboratories, Lucent Technology, 700 Mountain Avenue, Murray Hill, NJ 07974, USA*

³*Boriskov Institute of Catalysis, SB RAS, av. Lavrentieva 5, Novosibirsk 90, Russia 630090*

Abstract: Impurity atom cluster and nanocrystal formation in Er-implanted hexagonal SiC were studied using TEM and HAADF-STEM. Short interstitial loops were initially observed to form in the as-implanted layers. After annealing at 1600°C extended matrix defects (wide interstitial loops and voids), Er atom clusters and nanocrystals grew. The wide interstitial loops act as strong sinks capturing diffusing dopants that gather first in lines, then planes, and finally in three-dimensional ErSi₂ nanocrystals. The unstrained nanocrystals have a hill-like shape and only two polarity-dependent orientations with respect to the matrix. One-, two-, and three-dimensional Er atom clusters were also identified. For the case of Ge implantation, again the wide interstitial loops act as sinks for the implanted Ge, representing the seeds of the nanocrystal.

Key words: silicon carbide, Er implantation, ErSi₂ nanocrystals, high-resolution TEM, atomic resolution HAADF-STEM, EELS

INTRODUCTION

The properties of a material can be modified significantly if it is manipulated at the nanometer scale (Pavebi et al., 2000). SiC, which is a wide band gap semiconductor with outstanding electronic, optical, and mechanical properties (Choyke et al., 1997), is also a promising host material for a variety of nanocrystals. However, the number of techniques that can be used to form such nanostructures is restricted by the low diffusion coefficient of dopant atoms in SiC (Tairov & Vodakov, 1977). Possible candidates include molecular beam epitaxy (Fissel et al., 2000) and ion implantation (Heera et al., 2000*b*; Schubert et al., 2002). On the one hand, the dopant concentration must be high ($\sim 10^{20}$ cm⁻³)

to form nanocrystals by implantation, yet on the other hand, the resulting matrix damage may influence the optical and electrical properties of the matrix–nanocrystal system. The use of an elevated temperature during implantation helps to prevent amorphization due to transient enhanced diffusion (Heft et al., 1996; Usov et al., 1999; Janson et al., 2000). Defect-enhanced diffusion of the foreign atoms may then occur in the highly disturbed matrix due to the presence of long-range strain fields and dislocation cores (Fahey et al., 1989). Clustering of vacancies and void formation during annealing (Gorelik et al., 2002) may also create empty spaces for nanocrystal growth.

The control of the effects of clustering is thought to be the key to a successful implantation-based doping technology, where highly n- and p-type doped SiC is necessary for high power devices. Here clustering of the dopants has to be avoided (or at least controlled) as they can ultimately form

deactivating precipitates, reducing the net dopant concentration and, moreover, creating a brittle material (Choyke et al., 1994; Greulich-Weber, 1997).

The formation of nanocrystals such as Al (Lebedev et al., 1997; Usov et al., 1999), Al_4C_3 (Stoemenos et al., 1999; Heera et al., 2000a), BC (Bracht et al., 2000; Panknin et al., 2001), graphite and diamond (Heera et al., 2000b), hexagonal GeSi (Kaiser, 2001; Kaiser et al., 2003), and ErSi_2 (Kaiser et al., 2001) in SiC has been studied using high-resolution transmission electron microscopy (HRTEM). For the cases of Al, B, and C implantation, the process was not aimed at nanocrystal fabrication but rather occurred as the result of unwanted precipitate formation after high dose doping. The growth of interstitial loops in SiC after annealing has also been observed (Persson & Hultman, 2001), with nanocrystal growth occurring as a result of strain accommodation (Lebedev et al., 1997). However for Er, Ge, and Si implantation, the process is aimed at nanocrystal fabrication. In the case of Ge (Schubert et al., 2002) and Si nanocrystals, their future field of application is optoelectronics (Weissker et al., 2001), and the first evidence of the Quantum confinement has recently been reported in single hexagonal GeSi nanocrystals in hexagonal SiC (Bechstedt et al., 2002; Kaiser et al., 2002a). Transition metal precipitates created after high dose implantation may have interesting properties for spintronics (Shi et al., 1996).

Techniques for characterizing the electronic structure and local site symmetry of defects in SiC such as photoluminescence, infrared spectroscopy, electron paramagnetic resonance, X-ray spectroscopy, Rutherford backscattering, and deep level transient spectroscopy provide an ensemble average of the dopant properties. This is useful when one or two types of local arrangements dominate. When clustering occurs, the distribution of atoms becomes less homogenous and the interpretation of these methods becomes more complicated. Although the later stages of nanocrystal growth can be studied using HRTEM, this method fails for the identification of very small buried clusters (<1.5 nm or monolayer sheetlike clusters). Consequently, there is very little understanding of the early stages of how such precipitates nucleate and grow (Fahey et al., 1989).

As the atomic number of Er is much larger than that of Si or C, Er-implanted SiC is an ideal system for studying foreign atom location by TEM using Z-contrast imaging conditions (Crewe et al., 1970; Treacy et al., 1978). Using a field emission gun with an about one-atom wide beam in a scanning transmission electron microscope (STEM), a high-angle annular dark field (HAADF) signal can be recorded

on an atomic scale (Loane et al., 1988; Pennycook, 1989; Liu & Cowley, 1991). The electron energy loss spectrum (EELS) of the beam can be recorded simultaneously to determine the chemistry of an individual atomic column (Batson, 1993; Browning et al., 1993; Muller et al., 1993, 2000).

In the present study, the structure of high temperature, high dose Er-implanted 4H and 6H-SiC is studied before and after high temperature annealing. Er atom clusters as small as one atom column are imaged, and the nanocrystal formation in hexagonal SiC is discussed.

EXPERIMENTAL PROCEDURES

On-axis and 3.5° resp. 8° off-axis hexagonal SiC (6H resp. 4H) was implanted using 10^{16}-cm^{-2} 400-keV Er ions at 700°C , followed by thermal annealing for 3 min in an Ar atmosphere at 1600°C . Cross-sectional samples were prepared for TEM examination using mechanical polishing, dimpling, and low-angle Ar-ion milling. Selected specimens, especially for STEM work, were also prepared by tripod polishing. Microscopy was carried out using a JEOL 3010 equipped with a LaB_6 cathode using high angle centered dark field (HACDF; Kaiser & Chuvilin, 2003), high-resolution (HR) imaging, and energy dispersive X-ray (EDX) spectroscopy, and in a JEOL 2010F equipped with a field emission gun using EELS and HAADF-STEM. TEM lattice fringe spacings of the nanocrystals were measured to an accuracy of 0.2–0.5% using Digital Micrograph. The 0004 and 0006 reflections of the 4H-SiC and 6H-SiC matrix respectively were used as an internal calibration standard. Lattice plane bending maps were generated using the geometrical phase plug-in for Digital Micrograph (Hytch et al., 1998)

RESULTS AND DISCUSSION

Figure 1a shows a bright-field image of high dose Er-implanted 4H-SiC with a highly strained layer visible 70–170 nm below the sample surface. (This range agrees well with the one calculated for Er location by means of Monte Carlo simulations [80 and 170 nm] using the TRIM 95 code; Biersack & Ziegler, 1985.) Variations in contrast result mainly from the presence of short interstitial loops that are restricted by Frank-type partial dislocations closer to the surface, as well as from point defect clusters, which are further from the surface. The Er-EDX line profile overlaid

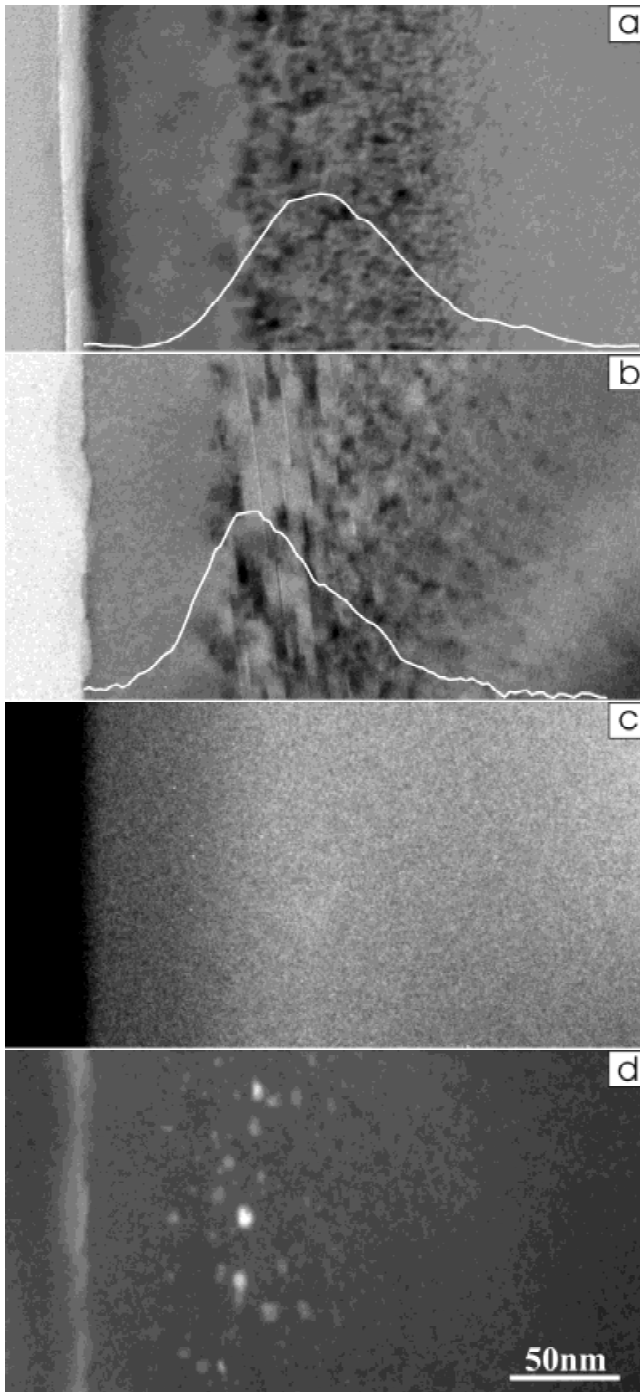


Figure 1. TEM images of Er-implanted SiC before (a) and (c) and after (b) and (d) annealing. Er-EDX line profiles are overlaid. a,b: (11-20) images. c,d: Incoherent dark-field images.

on the figure shows that the majority of the Er atoms are located in the strained layer. The corresponding HACDF image in Figure 1c shows the Er distribution in the form of bright spots with no significant clustering of either Er or vacancies.

After annealing at 1600°C, the matrix structure changes dramatically (just as for Ge implantation [Kaiser, 2001; Gorelik et al., 2002; Schubert et al., 2002]). In a bright-field image (Fig. 1b), the region further from the surface contains mottled contrast as in Figure 1a, whereas closer to the surface extended planar defects are seen. These defects are wide SiC interstitial loops. Their growth can be explained by the inward diffusion of Si and C interstitials as well as by Ostwald ripening (Ostwald, 1900). The maximum Er content is now shifted toward the surface and close to the middle of the layer containing the wide interstitial loops (Fig. 1b). The redistribution of Er into clusters is seen in the HACDF image in Figure 1d.

The vacancies condense after annealing and form voids in the surface region (0–70 nm from the surface). Moreover, the vacancy generation may be enhanced by the rough surface after Er ion bombardment and annealing (McCarty et al., 2001). The voids exhibit darker contrast in the Z-contrast dark-field (HAADF-STEM) image shown in Figure 2a, whereas Er agglomerates appear brighter within the SiC matrix. The voids, which are adjacent to the wide interstitial loops, are partly or completely filled with Er (see below). This observation and the shift of the Er profile toward the surface are attributed to the off-axis SiC material (which allows diffusion to take place along the wide interstitial loops to the void layer), and to the presence of Er in the region adjacent to the interstitial loops before annealing.

Figure 2b at higher magnifications shows bright clusters that have very different sizes, the largest of which are about 18 nm. The smallest clusters are seen in Figure 3 in the left two columns imaged in atomic resolution HAADF-STEM, and viewed along [11–20] projection in the 4H or 6H-SiC matrix. The high-spatial resolution EELS signal shown in Figure 4 obtained directly from the bright spot in the right upper HAADF-STEM image (corresponding to Fig. 3a, left image) shows the potential of the method to detect the chemistry of a single atom column and confirms that Er gives rise to the bright contrast. By tilting the specimen 30°, it is revealed that this is not a single Er atom but 4 Er atoms that have collected along the atom column (see the lower image on the right in Fig. 4). From the ADF contrast intensity seen in Figure 3, the number of Er atoms collected in the projected column is estimated to be between 4 and 10. The smallest clusters as well as the larger clusters (Fig. 3a–c, right) are connected to interstitial loops. Chains of Er atoms may be collected in the cores of dislocation segments of the wide interstitial loops, where the loop

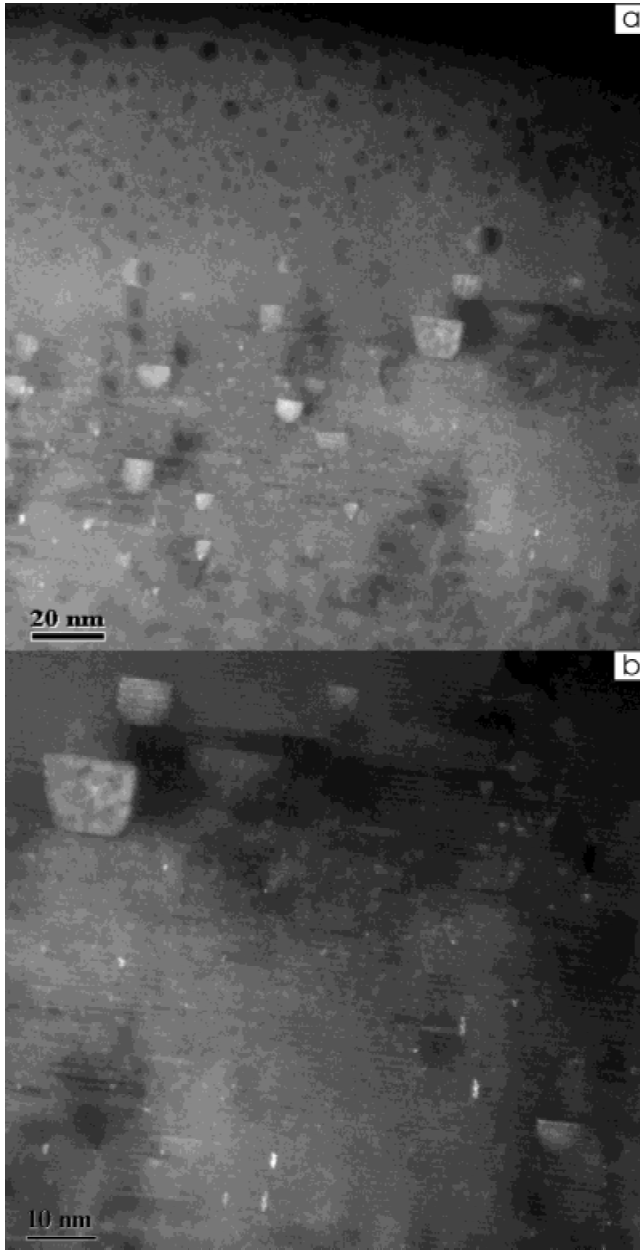


Figure 2. a: Low magnification xs-HAADF-STEM image showing dark voids and bright nanocrystals and small Er clusters. b: HAADF-STEM higher magnification image from a showing the small bright spots more clearly.

dislocation segments are located in neighboring (0001) planes in dipolelike configurations. The shift of the (0001) planes is clearer in high-resolution images of similar defects shown in the right images in Figure 3a–c. In Figure 3b, Er atom columns are seen to be lying in the (10–12) planes with an ABC stacking. Similar small prismatic defects were observed in {10–12} planes in 6H-SiC after high dose Xe irradiation (Lhermitte-Sebire et al., 1994). Er atoms were also found in

a more complicated defect configuration in the left two images of Figure 3c. As the strain around these defects is accommodated, these one- and two-dimensional clusters may be suggested as stable configurations. In Figure 3d irregular three-dimensional defect clusters containing chains of Er atoms are seen.

Figure 5 shows one-dimensional Er atom clusters that are parts of SiC interstitial loops that have bounding dislocations at their edges (left image) often in dipolelike configurations. However these clusters are not formed in neighboring (0001) planes, and, therefore, the surrounding strain field is not accommodated as visualized in the corresponding lattice plane bending map (middle image; Hytch et al., 1998) pointing to the origin of strain. As can be seen, only the HAADF-STEM image (Fig. 5b) shows that Er atoms are collected in the core regions of the edge dislocations. Although loops exist in the as-implanted sample as seen in the HRTEM image in Figure 6a (as marked), HAADF-STEM images show that they do not function as sinks for Er atoms during high-temperature implantation (Fig. 6b). Er is not clustered at the dislocation cores, but rather is randomly distributed (compare Fig. 1c).

As a result of local variations in Er concentration present in the TEM sample, different stages of nanocrystal formation can be observed in the same specimen. Figure 7 provides a snapshot of how the nanocrystals may be formed. The dislocation loops act as strong sinks capturing diffusing dopants, which gather first in lines, then planes, and finally in three-dimensional precipitates. Because of their long-range strain fields, chains of Er atoms in the cores of edge dislocations are considered nuclei for Er nanocrystal growth. Further migration of Er atoms and vacancies may be possible resulting finally in the growth of a new crystalline Er phase (Fig. 7c).

The peculiar feature of all nanocrystals, as well as the Er-containing sheets seen in Figure 7a,b, are their shapes. They are always found to be of hill-like shape as shown in Figure 8 and their orientation changes in response to the polarity of the SiC matrix. This strongly suggests that well-defined bonds between Er and the SiC matrix are formed. The sheetlike SiC Er cluster (Fig. 7a,b) seems to be a consequence of this chemical reaction. EELS measurements on the nanocrystals show that they contain both Er and Si.

Figure 9a,b shows high-resolution images of nanocrystals in 6H-SiC and 4H-SiC, respectively, and their diffractograms. The spacings of the lattice fringes show that the nanocrystals are unstrained ErSi_2 (P6mm). The orientation relationship is (depending on the polarity) 0001 (or 000-1)

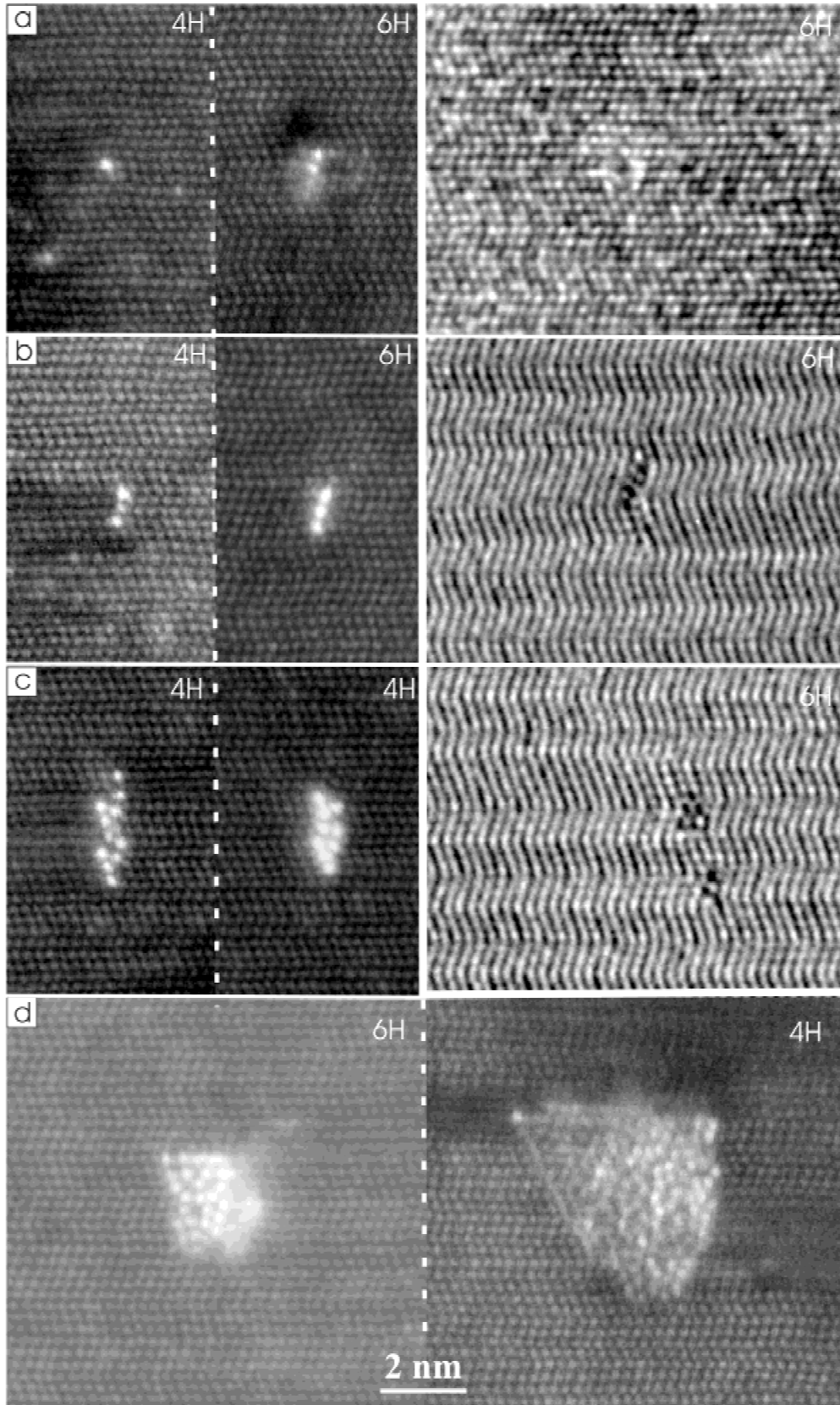


Figure 3. a–c: Atomic-resolution (11–20) HAADF-STEM images of Er atom clusters in 4H and 6H-SiC after Er-implantation and annealing in the left half of the figure. In the right half of the figure similar defects are imaged in high-resolution at [11–20] zone axis. d: Three-dimensional Er cluster in 6H and 4H-SiC imaged in HAADF-STEM.

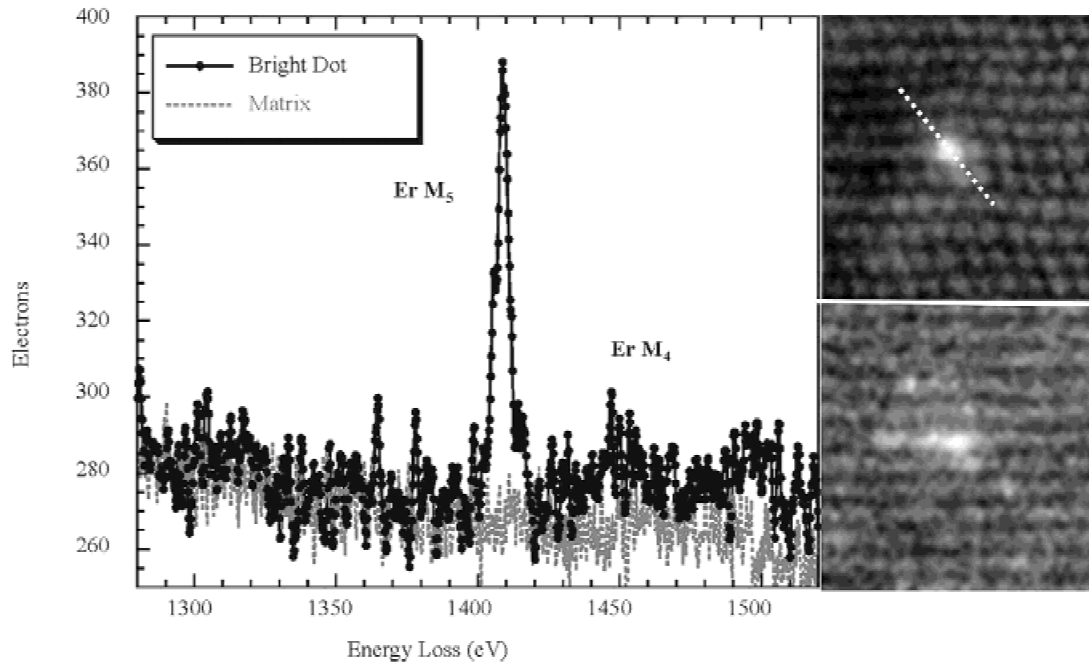


Figure 4. EELS spectrum obtained along the dashed line in the right upper HAADF-STEM [11-20] image. The right lower image shows the same defect in [01-10] projection. The individual atoms are not resolved in the latter projection but the projected length of 1 nm (giving a 2-nm actual length) and the Er-Er spacing of ~ 0.5 nm implies that there are about 4 atoms along the line.

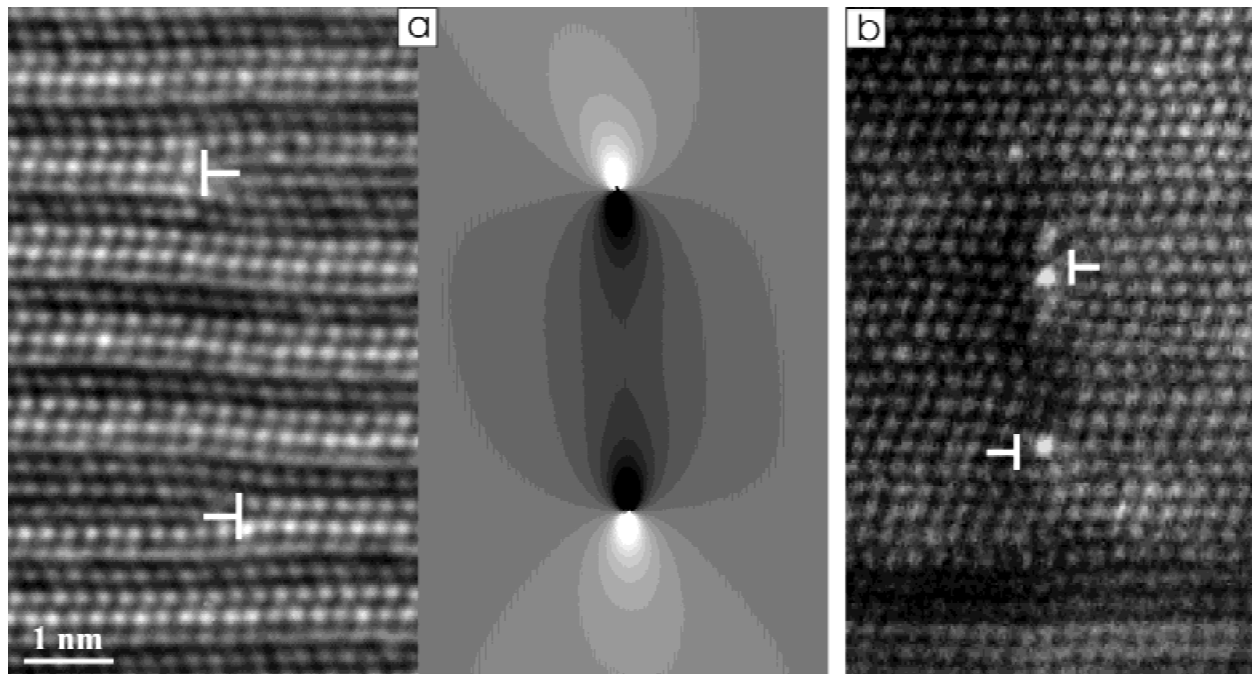


Figure 5. **a:** (11-20) high-resolution image of a defect found after annealing (the extra SiC planes are marked), and the corresponding lattice bending map. **b:** HAADF-STEM image of a similar defect.

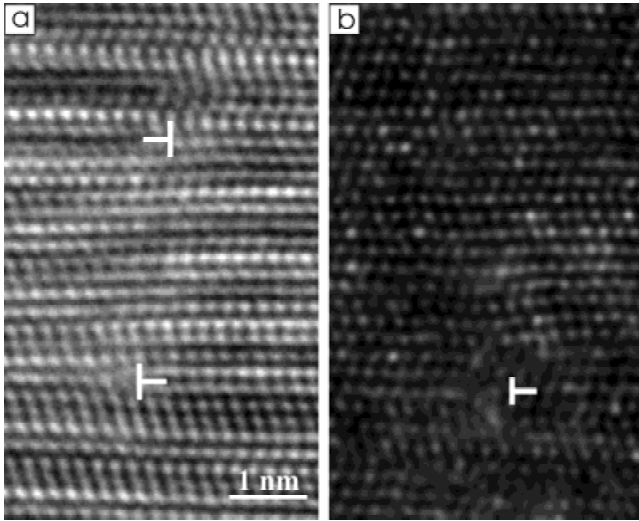


Figure 6. a: (11-20) high-resolution image of a defect found in the as-implanted specimen before annealing. b: HAADF-STEM image of a similar defect.

SiC // 0002 ErSi₂ and 01-10 SiC // 01-10 ErSi₂. In Figure 9a,b, the extra planes at the edges of the nanocrystals are seen by the bright-dark SiC contrast change (Kaiser et al., 1999) and are marked by arrows. The width between the interstitial loops in dipolelike configurations is typically between 3 and 5 times the c-lattice parameter of hexagonal SiC (1 nm for 4H-SiC; 1.5 nm for 6H-SiC). As such interstitial loops around the nanocrystals were generally found, the configuration in Figure 5 is suggested to be the seed of the nanocrystal. A similar correspondence between nanocrystal and interstitial loop location has been found for Ge implanted in hexagonal SiC at very similar implantation and annealing conditions. A high-resolution image of the nano-

crystal formed after Ge implantation is seen in Figure 10a in which a hexagonal GeSi nanocrystal (Kaiser, 2001) is viewed (the extra planes are marked by arrows). The bright spots in the HRTEM images in Figure 10b originate (in correspondence to the Er case) from Ge atoms that segregated near the cores of the dislocation segments as was shown by HAADF-STEM. However, the Ge atoms have a far more complicated arrangement around the core compared to the simple chainlike structure of the Er atoms inside the dislocation core (Kaiser et al., 2002b). This may be related to a different site preference for Er and Ge atoms, as well as the tendency for Ge to form precipitates that have smaller surface/volume ratios than Er (suggesting a higher interface energy). From our observation, it may be concluded that the dislocation loops form before the nanocrystals. In contrast, for high dose Al implantation and annealing it has been suggested that loops form as a consequence of nanocrystal formation (Lebedev et al., 1997).

Figure 11, which was obtained adjacent to the interstitial loop region (see Fig. 2), shows that ErSi₂ nanocrystal also forms in the region where no interstitial loops are present. The void formation can be explained by defect clustering during the flow of vacancies toward the surface (Fahey et al., 1989). Because ErSi₂ partly filled the voids, this strongly suggests a connection between vacancy clustering, Er inward diffusion, and the chemical reaction between Er and Si, as in the case of the wide interstitial loops. The bright-field and incoherent dark-field images seen in Figure 11a,b show that even when the nanocrystals do not grow as large as the voids, the internal surface of the voids is covered by Er. Figure 11c,d shows corresponding high-resolution images. The ErSi₂ nanocrystals that form inside the voids have the same lattice parameters, the same orien-

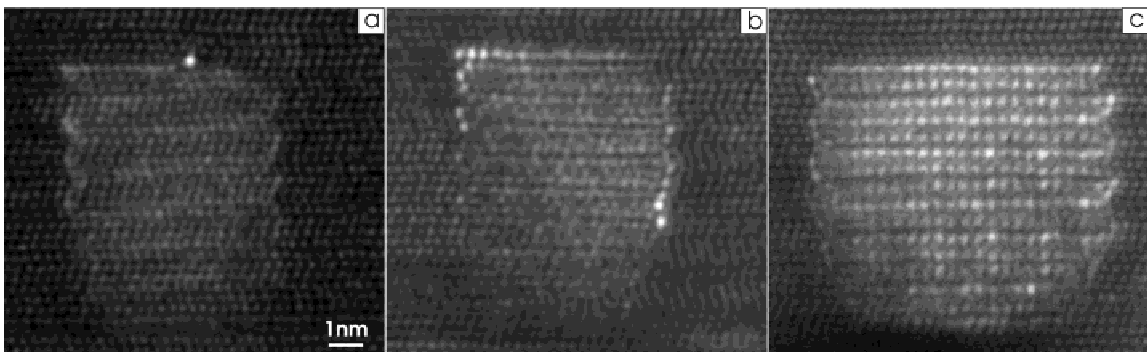


Figure 7. a–c: Atomic-resolution (11-20) HAADF-STEM images of different stages of nanocrystal formation in 4H-SiC.

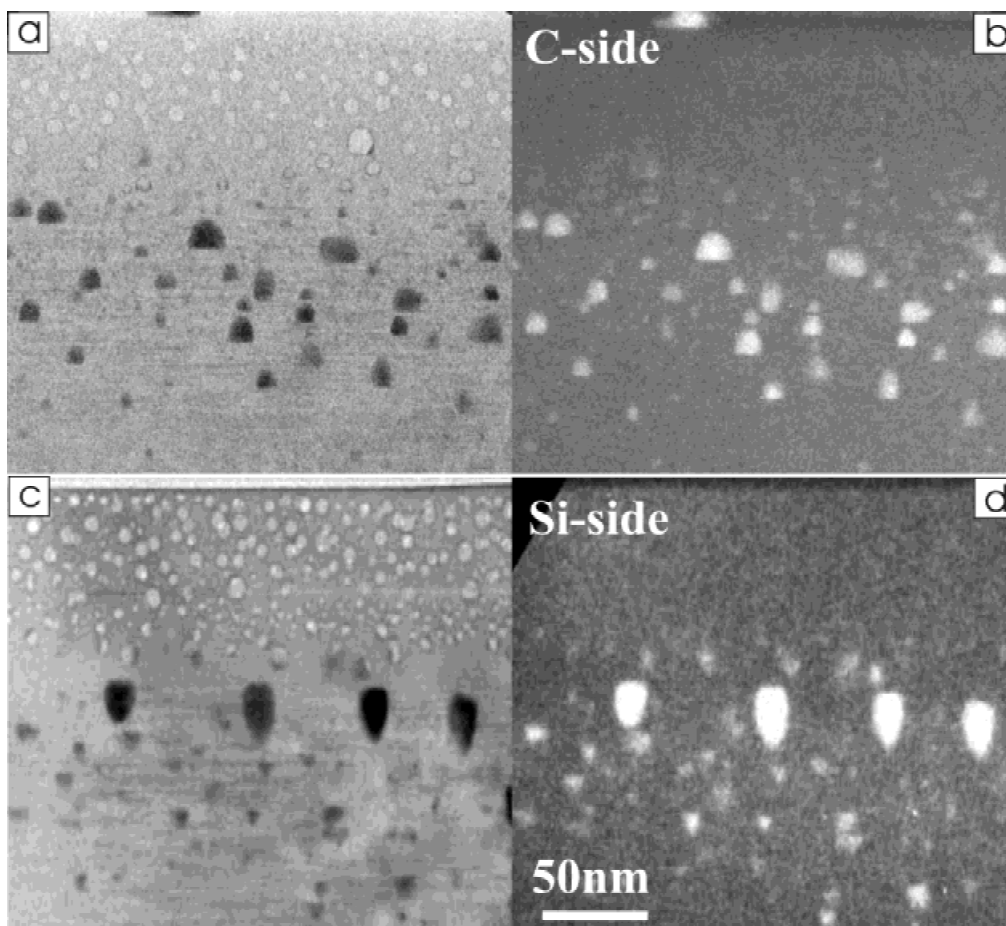


Figure 8. **a,c:** Underfocused bright-field images. **b,d:** Incoherent dark-field images showing voids and nanocrystals after Er implantation into the (000-1) SiC (C-side) and (0001) SiC (Si-side) surface. Note the different orientation of the hill-shaped nanocrystals toward the specimen surface.

tation relationship to the SiC matrix, and the same hill-like shape as the nanocrystals that form at the interstitial loops.

SUMMARY AND CONCLUSION

Er atom cluster and ErSi_2 nanocrystal growth after high dose Er-ion implantation of hexagonal SiC has been studied using TEM. Defects consisting of short interstitial loops are seen before annealing. However, even at an elevated implantation temperature of 700°C , they do not act as sinks for Er or for vacancies. After annealing at 1600°C , nanocrystals form as a result of defect annihilation, activated possibly by strains around the edges of the wide SiC interstitial loops or

by void formation during surface-directed vacancy migration. Er atoms inside the core of the edge dislocation are suggested to be the seed of the nanocrystal. The nanocrystals are unstrained hexagonal ErSi_2 , hill-shaped, and with two well-defined polarity-dependent orientation relationships with the matrix. In contrast, GeSi nanocrystals do not undergo a chemical reaction, are faceted, and are found in a variety of orientational relationships (Kaiser, 2001). Nevertheless, and parallel to the Er case, Ge is captured at the edges of interstitial loops and GeSi nanocrystals are similarly connected with them, suggesting that first the interstitial loop and then the nanocrystals have been formed. Special small treelike Er-atom clusters in (10–12) planes were also found; their exact defect description and formation kinetics are a matter of ongoing work.

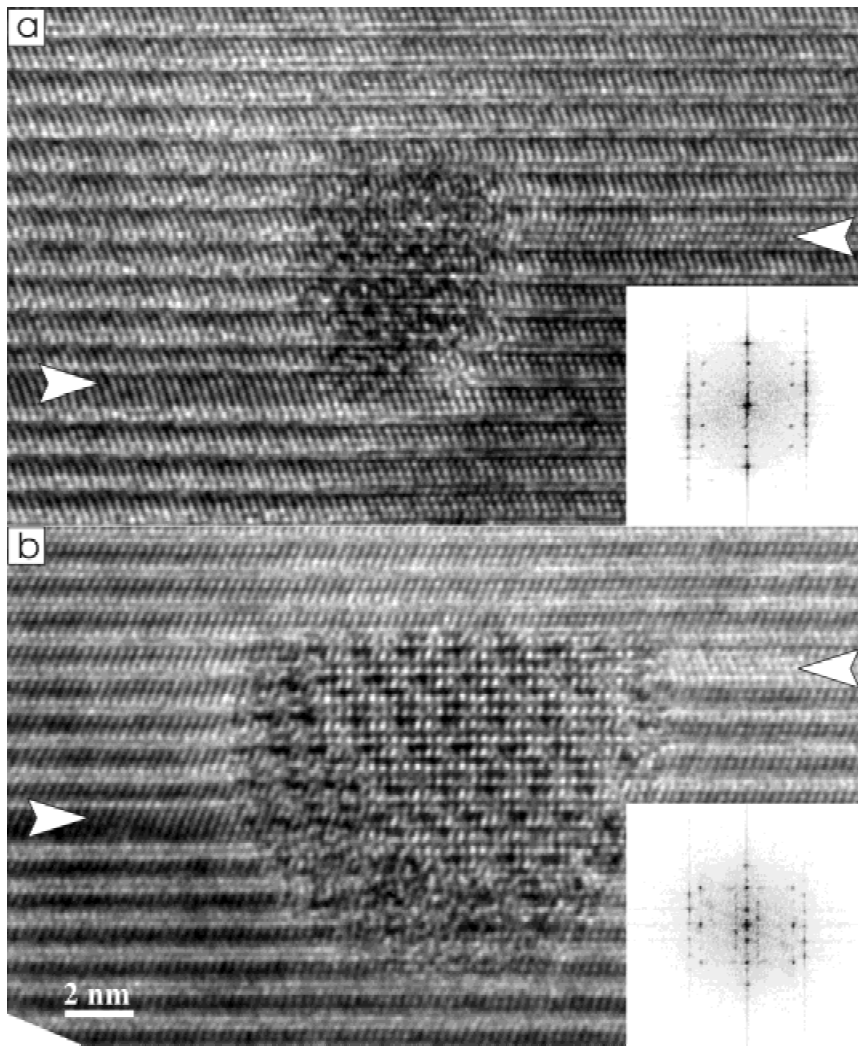


Figure 9. (11-20) high-resolution images of ErSi_2 nanocrystals and corresponding diffractograms. Interstitial loops (marked by arrows) are arranged in dipolelike configurations around the nanocrystals (a) in 6H-SiC, (b) in 4H-SiC.

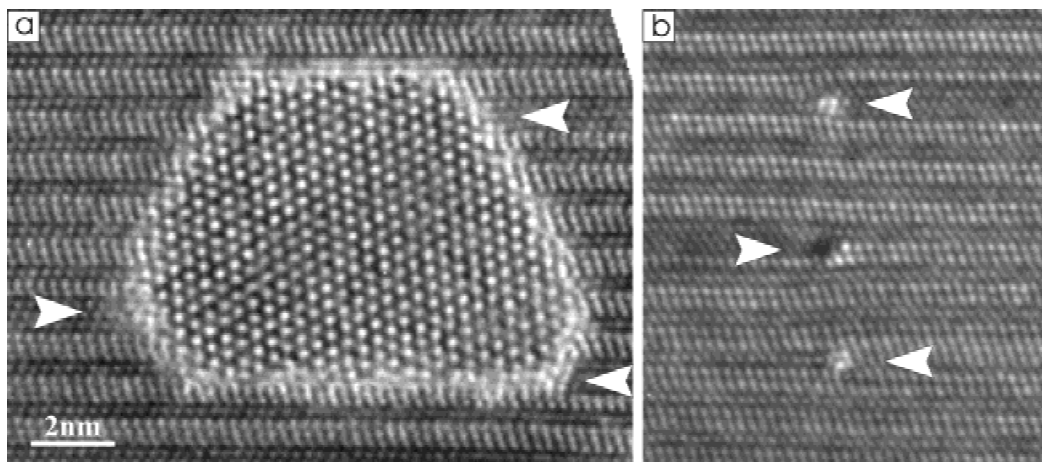


Figure 10. (11-20) high-resolution images obtained after Ge implantation and annealing showing a very similar location of interstitial loops around the GeSi nanocrystal (a) and around a defect without nanocrystals (b). The bright spots at the edges of the interstitial loops can be explained by Ge agglomeration acting as the seed of the nanocrystal (Kaiser et al., 2002b).

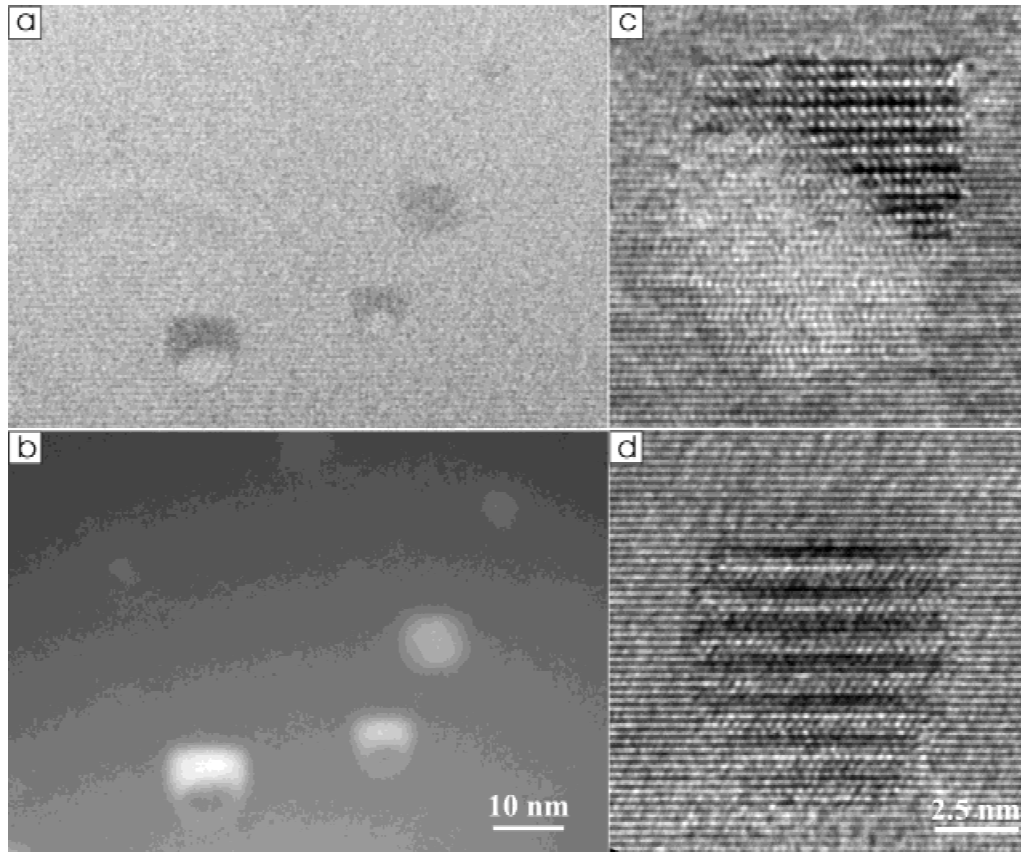


Figure 11. Bright field (a) and incoherent dark-field (b) images obtained from partly and fully filled voids (with ErSi₂) in the region adjacent to the wide interstitial loops. c,d: High-resolution images of ErSi₂ formed inside the voids.

ACKNOWLEDGMENTS

We are grateful to Prof. Jim Choyke and to Dr. Igor Khodos for helpful discussions and to Prof. Jim Choyke for the supply of the high quality SiC material. We thank Istvan Kovacz and John Grazul for TEM sample preparation. We acknowledge the Ge-ion implantation by Chr. Schubert. This work has been supported by the German Research Foundation (DFG), Sonderforschungsbereich 196.

REFERENCES

- BATSON, P.E. (1993). Simultaneous STEM imaging and electron energy-loss spectroscopy with atomic column sensitivity. *Nature* **366**, 727–728.
- BECHSTEDT, F., FISSEL, A., GROSSNER, U., KAISER, U., WEISSKER, H.-C. & WESCH, W. (2002). Towards quantum structures in SiC. *Mat Sci Forum* **389–393**, 120–125.
- BIERSACK, J.P. & ZIEGLER, J.F. (1985). *The Stopping and Ranges of Ions in Matter*. Vol. 1, Pergamon Press.
- BRACHT, H., STOLWIJK, N.A., LAUBE, M. & PENSL, G. (2000). Diffusion of boron in silicon carbide: Evidence for the kick-out mechanism. *Appl Phys Lett* **77**, 3188–3190.
- BROWNING, N.D., CHISHOLM, M.M. & PENNYCOOK, S.J. (1993). Atomic-resolution chemical analysis using a scanning transmission electron microscope. *Nature* **366**, 143–146.
- CHOYKE, W.J., DEVATY, R.P., CLEMEN, L.L. & YOGANATHAN, M. (1994). Intense erbium-1.54- μm photoluminescence from 2 to 525 K in ion-implanted 4H, 6H, 15R and 3C SiC. *Appl Phys Lett* **65**, 1668–1670.
- CHOYKE, W.J., MATSUNAMI, H. & PENSL, G. (1997). *Silicon Carbide*. Berlin: Wiley-VCH.
- CREWE, A.V., WALL, J. & LANGMORE, J. (1970). Visibility of single atoms. *Science* **168**, 1338–1340.
- FAHEY, P.M., GRIFFIN, P.B. & PLUMMER, J.D. (1989). Point defects and dopant diffusion in silicon. *Rev Modern Physics* **61**, 289–384.
- FISSEL, A., SCHRÖTER, B., KAISER, U. & RICHTER, W. (2000). Advances in the molecular-beam epitaxial growth of artificially layered heteropolytypical structures of SiC. *Appl Phys Lett* **77**, 2418–2420.
- GORELIK, T., KAISER, U., SCHUBERT, CH., WESCH, W. & GLATZEL,

- U. (2002). A TEM study of Ge implanted into SiC. *J Mater Res* **17**, 479–486.
- GREULICH-WEBER, S. (1997). EPR and ENDOR investigations of shallow impurities in SiC polytypes. *Phys Stat Sol (A)* **162**, 95–151.
- HEERA, V., REUTHER, H., STOEMENOS, J. & PECZ, B. (2000a). Phase formation due to high dose aluminium implantation into silicon carbide. *J Appl Phys* **87**, 78–85.
- HEERA, V., SKOPURA, W., PECZ, B. & DOBOS, L. (2000b). Ion beam synthesis of graphite and diamond in silicon carbide. *Appl Phys Lett* **76**, 2847–2849.
- HEFT, A., WENDLER, E., HEINDL, J., BACHMANN, T., GLASER, E., STRUNK, H.P. & WESCH, W. (1996). Damage production and annealing of ion implanted silicon carbide. *Nucl Instrum Meth B* **113**, 239–243.
- HYTCH, M.J., SNOECK, E. & KILAAS, R. (1998). Quantitative measurement of displacement and strain fields from HREM micrographs. *Ultramicroscopy* **74**, 131–146.
- JANSON, M.S., LINNARSSON, M.K., HALLEN, A. & SVENSSON, B.G. (2000). Transient enhanced diffusion of implanted boron in 4H-silicon carbide. *Appl Phys Lett* **76**, 1434–1436.
- KAISER, U. (2001). Nanocrystal formation in hexagonal SiC after Ge ion implantation. *J Electr Microsc* **50**, 251–263.
- KAISER, U., BISKUPEK, J. & GÄRTNER, K. (2003). Faulted GeSi and Si nanocrystals buried in hexagonal SiC. *Phil. Mag Lett* **83**, 253–263.
- KAISER, U., BISKUPEK, J., MULLER, D., GÄRTNER, K. & SCHUBERT, CHR. (2002a). Properties of GeSi nanocrystals embedded in hexagonal SiC. *Cryst Res Technol* **37**, 392–406.
- KAISER, U. & CHUVILIN, A. (2003). On the reveal of crystalline precipitates within a crystalline matrix using CTEM. *Microsc Microanal* **9**, 36–41.
- KAISER, U., CHUVILIN, A. & RICHTER, W. (1999). On the peculiarities of bright/dark contrast in HRTEM images of SiC polytypes. *Ultramicroscopy* **76**, 21–37.
- KAISER, U., CHUVILIN, A., RICHTER, W., PASOLD, G., WITTHUHN, W., SCHUBERT, CHR., WESCH, W. & CHOYKE, J.W. (2001). Nanocrystal formation after Er implantation in 6H-SiC. *Proceedings Widegap 2001*, Exeter, UK. J. Phys.: Condensed Matter.
- KAISER, U., MULLER, D.A., GRAZUL, J.I., CHUVILIN, A. & KAWASAKI, M. (2002b). Atomic-scale studies of the nucleation and growth of nanocrystals after ion implantation. *Nature Materials* **1**, 102–105.
- LEBEDEV, O.I., VAN TENDELOO, G., SUVOROVA, A.A., USOV, I.O. & SUVOROV, A.V. (1997). HREM study of ion implantation in 6H-SiC at high temperatures. *J Electron Microsc* **46**, 271–279.
- LHERMITTE-SEBIRE, I., VICENS, J., CHERMANT, J.L., LEVALOIS, M. & PAUMIER, E. (1994). Transmission electron microscopy and high-resolution electron microscopy studies of structural defects induced in 6H-SiC single crystals irradiated by swift Xe ions. *Phil Mag A* **69**, 237–244.
- LIU, J. & COWLEY, J.M. (1991). Imaging with high-angle scattered electrons and secondary electrons in STEM. *Ultramicroscopy* **37**, 50–71.
- LOANE, R.F., KIRKLAND, E.J. & SILCOX, J. (1988). Visibility of single heavy atoms on thin crystalline silicon in simulated annular dark field. *Acta Cryst A* **44**, 912–927.
- MCCARTY, K.E., NOBEL, J.A. & BARLETT, N.C. (2001). Vacancies in solids and the stability of surface morphology. *Nature* **412**, 622–625.
- MULLER, D.A., SORSCH, T., MOCCIO, S., BAUMANN, F.H., EVANS-LUTTERODT, K. & TIMP, G. (2000). The electronic structure at the atomic scale of ultrathin gate oxides. *Nature* **399**, 758–761.
- MULLER, D.A., TZOU, Y., RAJ, R. & SILCOX, J. (1993). Mapping sp^2 and sp^3 states of carbon at sub-nanometer spatial resolution. *Nature* **366**, 725–727.
- OSTWALD, W. (1900). Über die vermeintliche Isomerie des roten und gelben Quecksilberoxyds und die Oberflächenspannung fester Körper. *Z Phys Chem* **34**, 495–503.
- PANKNIN, D., WIRTH, H., MÜCKLICH, A. & SKORUPA, W. (2001). Electrical and microstructural properties of highly boron-implantation doped 6H-SiC. *J Appl Phys* **89**, 3162–3167.
- PAVEBI, L., DALNEGRO, L., MOZZOLENI, C., FRANCO, G. & PRIOLO, F. (2000). Optical gain in Si nanocrystals. *Nature* **408**, 440–445.
- PENNYCOOK, S.J. (1989). Z contrast STEM for materials science. *Ultramicroscopy* **30**, 58–69.
- PERSSON, P.O.A. & HULTMAN, L. (2001). Growth evolution of dislocation loops in ion implanted 4H-SiC. *Mat Sci Forum* **353–356**, 315–318.
- SCHUBERT, CH., KAISER, U., HEDLER, A., WESCH, W., GORELIK, T., GLATZEL, U., KRÄUSSLICH, J., WUNDERLICH, B., HESS, G. & GOETZ, K. (2002). Nanocrystal formation in SiC by Ge ion implantation and subsequent thermal annealing. *J Appl Phys* **91**, 1520–1524.
- SHI, J., GIDER, S., BABCOCK, K. & AWSCHALOM, D.D. (1996). Magnetic clusters in molecular beams. *Met Semicond Sci* **271**, 937–941.
- STOEMENOS, J., PECZ, B. & HEERA, V. (1999). Epitaxial aluminium carbide formation in 6H-SiC by high-dose Al^+ implantation. *Appl Phys Lett* **74**, 2602–2604.
- TAIROV, Y.M. & VODAKOV, Y. (1977). *A 2.Group IV Materials “Electroluminescence,”* J.I. Pankove (Ed.), p. 35. Berlin, Heidelberg: Springer Verlag.
- TRACY, M.M.J., HOWIE, A. & WILSON, C.J. (1978). Z contrast of platinum and palladium crystals. *Phil Mag A* **38**, 569–585.
- USOV, I.O., SUVOROVA, A.A., SOKOLOV, V.V., KUDRYAVTSEV, Y.A. & SUVOROV, A.V. (1999). Transient enhanced diffusion of aluminium in SiC during high temperature ion implantation. *J Appl Phys* **86**, 6039–6042.
- WEISSKER, H.C., FURTHMÜLLER, J. & BECHSTEDT, F. (2001). First-principles of optical properties: Application to embedded Ge and Si dots. *Phys Stat Sol B* **224**, 769–773.